An Electrohydrodynamic Thermal Convective Gyroscope based on Ion Wind Corona Discharge

Ngoc Tran Van[1], Tung Thanh Bui[2], Canh-Dung Tran[3], Thien Xuan Dinh[4], Hoa Phan Thanh[5], Trinh Chu Duc[2] and Van Thanh Dau[6]

[1]Institute of Missile – Academy of Military Science and Technology, Vietnam

[2]VNU University of Engineering and Technology, Vietnam National University, Hanoi, Vietnam

[3]School of Science and Engineering, Ritsumeikan University, Shiga 525-8577, Japan

[4]School of Mechanical and Electrical Engineering, University of Southern Queensland, Queensland QLD 4350, Australia

[5]Department of Electronic and Energy Engineering, Hanoi University of Industry, Hanoi, Vietnam

[6]School of Engineering and Built Environment, Griffith University, Queensland QLD 4222, Australia

Abstract

A novel configuration of gyroscope using an electro-hydrodynamics flow circulating in a confined space is developed. The configuration includes three corona discharge based actuators to generate ionic flows inside three separated sub-channels which are connected to the main chamber. Ionic flows are merged together while they move through a nozzle installed at the main chamber entrance. After the merging phase, the conflated flow is diverged to move back to sub-channels where each accelerates at the discharge actuator. A master ring is installed at the end of the nozzle to remove any residual charge of the conflated ion flow. The ion flow velocity is measured using several hotwires installed in the main chamber. Since the configuration does not require any vibrating components, the present device is robust, cost-effective and consumes low power, hence, very potential in application of inertial sensing.

Keywords: thermal convective gyroscope, ion wind, electrohydrodynamic

1. Introduction

Circulatory flow in a confined space has been applied in the inertial sensing and particularly in the angular rate sensing where the advantage of self-contained valveless micropump reduces the risk of damage to mechanical counterparts [1]–[3]. For those devices, it is necessary to create a jet flow within the system. Several techniques were developed to generate a jet flow, for example the vibration methods using a lead zircona-titanate (PZT) diaphragm [4]–[9], activating a jet flow by electrohydrodynamics in a high electric field using an electro-conjugate fluid [10], by the natural convection from a locally heated region where the flow moves along the direction of mass diffusion [11], or by thermal expansion of gas to move air flow from an expansion state to a diffusion one [12].

Recently, our group has developed an open-space jet flow gyroscope with regard to the advantages of a corona-discharge in which ion wind is generated by a high–voltage applied between a pin, as the discharge electrode, and a ring, as the reference electrode [13]. For such configuration, the induced Coriolis force deflects the ion wind and the gyroscope detects the angular rate of the system. This ion wind based devices possess several advantages including lower cost and energy consumption, tidy and light but solid structure owing to no moving parts and simple operation compared with those by other methods using air pumps or oscillating pistons [14]–[16].

Our recent experiments have found that the introduction of this idea into a closed system yields more many advantages, especially in avoiding the influence of surrounding environment and increasing the capability and efficiency of the systems [17], [18]. Furthermore, by this idea jet flow in generators can be designed using different configurations of electrodes, for example, with the needle-to-ring or with dual-needle configuration [19]. However, the circulartory ionic wind is transiently unstable due to the accumulation of the residual electric charge in closed systems, which damages the corona discharge process. In order to overcome these barriers, the ion wind based closed system using a new configuration of multiple pin-ring electrodes was introduced [20], and is further developed in this work. For the present approach, a master ring is introduced into the system at the working channel to neutralize the residual charge. The new configuration based device is experimentally investigated and sufficiently evaluated, and an application of the present device in sensing angular rate is demonstrated.

2. Mechanism and design of device

2.1. Mechanism of the device

A flow network operates in the axisymmetric device consisting of three cylindrical chambers (ion wind chambers) which are connected together before linked with a working/sensing chamber through a nozzle at the device center where hotwires are installed (see Fig. 1(a)). The dimensions (described by diameter × length) of the ion wind and working cylindrical chambers are 5 mm × 10 mm and 12 mm × 15 mm, respectively as designed in the simulated model.

In each ion wind chamber, a pin-ring configuration is installed and plays the role of an actuator of ion wind. The pin of 0.4 mm diameter with a spherical tip of 80 µm radius is located at an optimized distance from the ring. The pin length of 8 mm is chosen for the sake of easy assembly of the device. The ring dimensions are 6 mm × 10 mm × 0.1 mm (inner diameter × outer diameter × thickness). A big ring named as master ring is set up in the sensing chamber. All rings and pins are made by stainless steel SUS304.

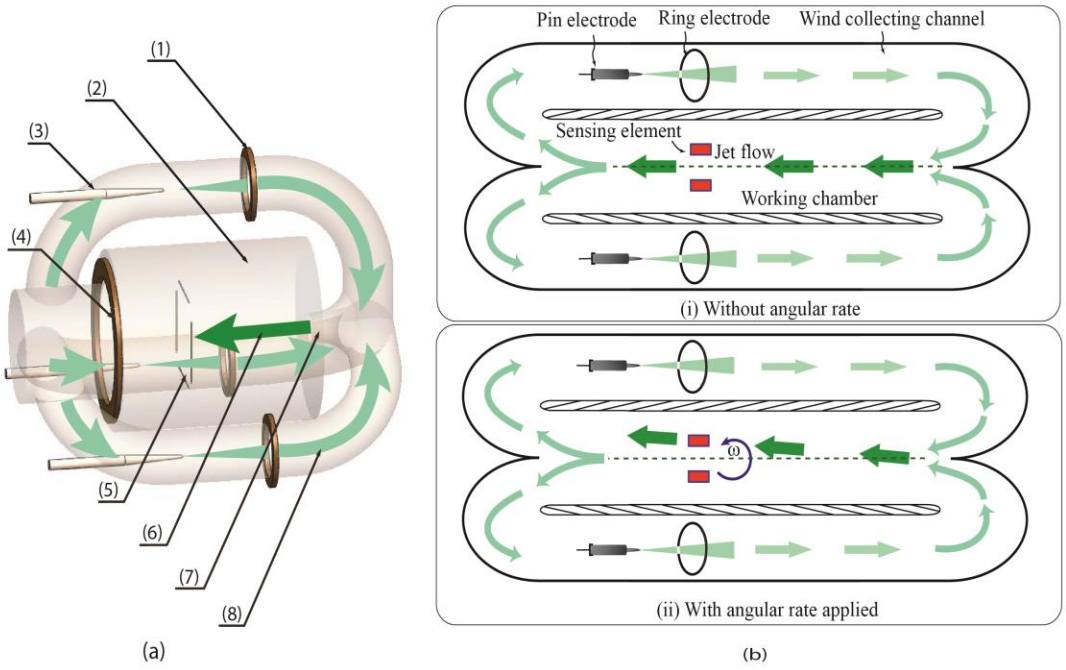

Figure 1. (a) Schema of the present device: (1) ring electrode, (2) working chamber, (3) pin electrode, (4) master ring electrode, (5) sensing element, (6) jet flow, (7) nozzle and (8) wind collecting channel; (b) ionic wind inside flow in cases of with and without applied angular rate

By a high voltage applied between pin-ring electrodes (1)&(3), ion winds generated in the three ion wind channels (8) drive air in chambers (8) moving toward a nozzle (7) where the conflated jet flow (6) propagates into the working chamber (2) before it is separated into the three ion wind chambers where each accelerates. Such repeated process of merging and separation of flows creates a circulating flow inside the system as described in Fig. 1. After each cycle of the propagation, the velocity of airflow through the working chamber gradually increases until reaching a stable state.

As we have known, the integration of ion winds into the circulatory airflow produces the residual electric charge in the closed system. This yields a reserved electrical field and then causes critical damage to the corona discharge process. Thus, a grounded master ring (4) is installed inside the working chamber (2) to neutralize the conflated flow before it is separated and return into ion wind channels.

Inside the working chamber, the Coriolis acceleration by the rotation of the turntable deflects. This deflection of airflow is detected using a sensing element of hotwires (5) installed on a plane located at a distance *L* from the nozzle (see Fig. 1(a)). The deflection of flow (d_ω) can be determined as follows.

$$\left|\overrightarrow{d_\omega}\right| = \left|\iint \overrightarrow{a_\omega} dt\right| = \left[\iint 2\vec{U} \times \vec{\omega} dt\right] = \omega L^2/U, \quad (1)$$

where $\overrightarrow{a_\omega}$ is the Coriolis acceleration, *U* the average velocity of ion wind, ω the angular velocity of turntable and *L* the distance from the sensing element of hotwires to the nozzle.

Let β be the gradient of the velocity of air flow going through the plane of sensing element, the deflection of air flow (ΔU_ω) can be converted into a variation of air flow velocity as follows.

$$\Delta U_\omega = \beta \cdot d_\omega = \beta\omega \frac{L^2}{U} \quad (2)$$

The average velocity of ion wind is estimated based on the discharge current as $U = k\sqrt{I/\rho\mu}$ ([21]) where, μ = 1.6×10^{-4} m^2·V^{-1}·s^{-1} is the ion mobility, ρ = 1.2041 kg·m^{-3} the air density, *I* the discharge current in μA, and *k* a coefficient and depends on the electrode discharge area and the inter-electrode distance.

For the similar inter-electrode distance as mentioned in [22], *k* is 0.014 m$^{-1/2}$ and thus,

$$\Delta U_\omega \approx (\beta\omega L^2/\mathrm{k})\sqrt{\rho\mu/I} \quad (3)$$

This velocity variation of airflow yields a difference of the temperatures and then the resistances of hotwires.

2.2. Experimental set-up

A prototype of the present device as designed was manufactured using 3D printer as shown in Fig. 2(a). In the working chamber, hotwires by tungsten whose resistance and temperature coefficient of resistance (TCR) are 3.4 (±0.3) Ω and 4500 ppm/°C, respectively each is installed in a plane located at a distance (L) of 7 mm away from the nozzle as shown in Fig. 1a. On this plane, the hotwires are equally positioned 2.5 mm from the center of the working chamber. The hotwires are connected to an electric circuit (Fig. 2) to capture and record signals generated by the voltage variation on hotwires using Memory HiLogger LR8400-20 (Hioki - Japan). A high voltage source by Glassman EH10R10 is applied between pin-ring electrodes as presented in Fig. 2a to generate ion winds inside wind collecting channels, and microampere meters M244T41 are set up to measure the discharge current variation of the system.

The capability of the present device to detect angular rate is investigated using the turntable system by Acutronic Ltd. The device is mounted at the center of a turntable (see Fig. 2b). In order to facilitate the transmission of electrical power and signals from outside to the device while the table is rotating, slip-rings are used to connect the device to electrical source and other parts of the system.

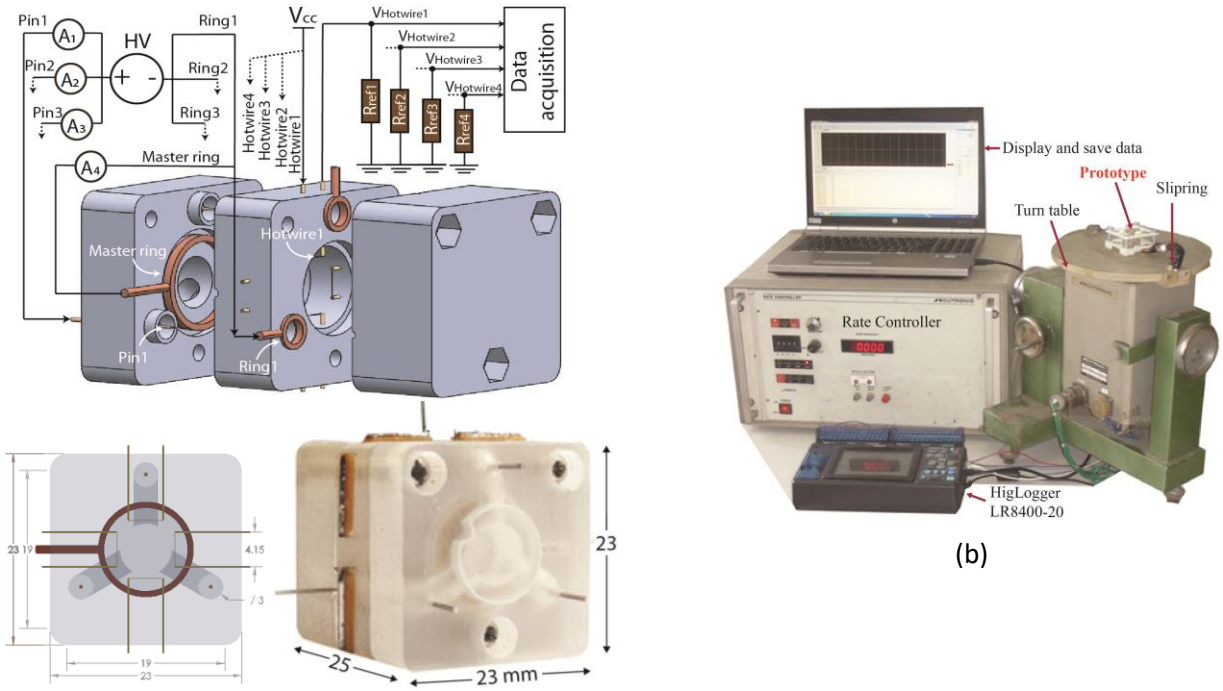

Figure 2. Experimental work. (a) Designed sensor with schema of measurement setup (i) and fabricated prototype (ii); and (b) Measurement system to detect flow deflection by a sensing element of hotwires using a turntable.

3. Experiment results and discussion

3.1. I–V characteristics of corona discharge

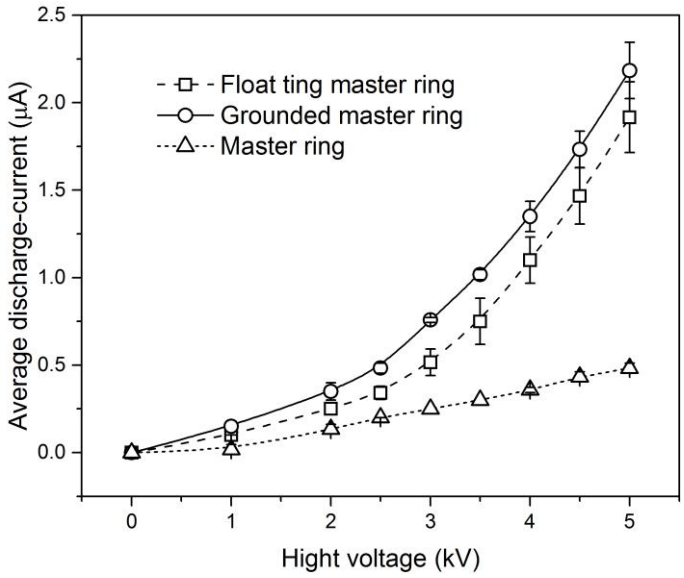

Figure 3. Current-Voltage (I-V) characteristics of the system: 1) I–V characteristic by all three pairs of pin-ring electrodes inside ion wind chambers with grounded master ring (circle marker) and floating master ring (square marker), and 2) I-V characteristic of mastering (triangle marker).

The current-voltage (I-V) characteristics of the system were established by the experiment as shown in Fig. 3 in which the voltages by all three pairs of pin – ring electrodes are plotted versus the current (I) while the master ring is floating (square maker line) or connected with ground (circle marker line). In the case of floating master ring, the I-V characteristic of master pin-ring electrodes (triangle marker line) is also observed. Results showed that for both cases of the master ring, the discharge current increases with the increase of the voltage applied on pin electrodes. Particularly, the discharge current with respect to the voltage (top curve) by the all three pin-ring electrodes is equal to the sum of discharge currents measured at each pair of pin-ring electrodes installed in ion wind channels. Furthermore, the I-V characteristics of three pairs of pin-ring electrodes presented by the three bottom curves are almost coincident. If the master ring is grounded, a residual charge carried by the ion wind in working chamber moves through the master ring. This part of current is evidenced by the ~~diminution~~ of the system discharge current in comparison with one in the case of the master ring connected to ground. The discharge current of system ~~decreased~~ with the increase of voltage applied on master ring electrode.

3.2. Performance of hotwires

Experimental results by Fig. 4 depict that the output voltage measured on hotwires increases with the increase of applied voltage on pin-ring electrodes. This can be explained by the increase of ion wind ~~corona discharge with respect to voltage~~, which accelerates ~~airflow moving through hotwires and strengthens the~~ thermal convection between hotwires and airflow. It yields a quick decrease of the hotwire temperature and change the voltage on hotwires (U_{hw}). In addition, experimental observation found that the output voltage on hotwires does not change until the voltage applied between pin-ring electrodes reached 2 kV.

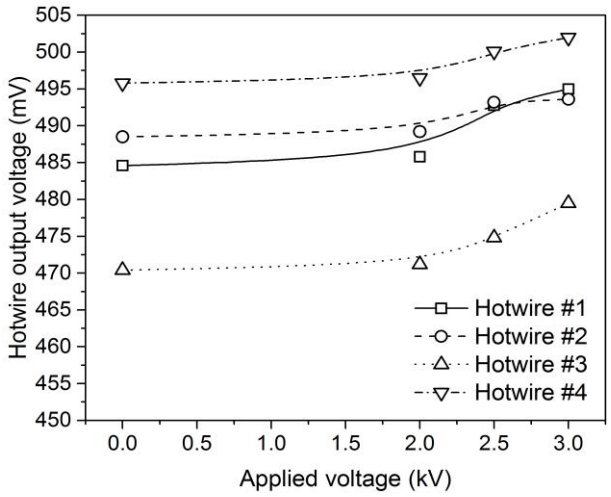

Figure 4. Experimental results: Output voltage measured on four hotwires plotted versus the applied voltage with the floating master ring. Hotwires are heated with a current of 100 mA.

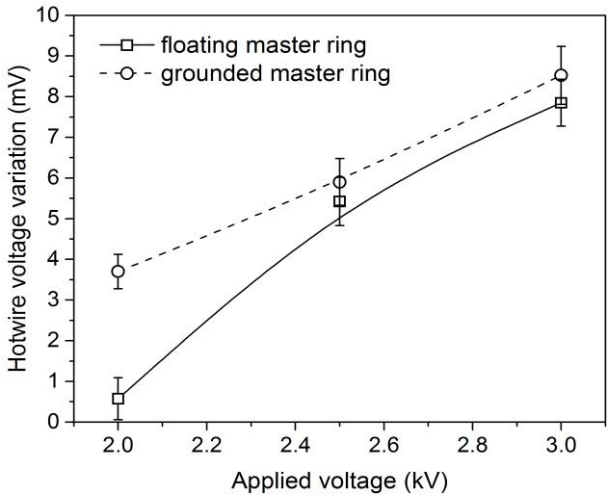

Figure 5. Experimental results: Average output voltage measured on four hotwires plotted versus the applied voltage while the master ring is activated (circle line) by a high voltage or inactivated (square line). Error bars are the two standard deviations from the means, account for 95.45% measuring confidence. The outputs were offset from their initial value when high voltage is off.

In order to illustrate the characteristic of the new configuration, the output voltage on hotwires ~~is observed~~ for two cases of the grounded and floating master rings. The average output voltage measured on four hotwires together with its deviation bar plotted versus the applied voltage in Fig. 5 shows a significant impact of the master ring on ion wind and then on the air velocity inside the working chamber. With a given applied

voltage, the intensity of ion wind is stronger if the master ring is activated, i.e. it is grounded. Furthermore, while the characteristic of the present configuration is linear with grounded master ring (circle line), it is nonlinear for floating one (square line).

3.3. Application in sensing angular rate

For this application, the present device is horizontally installed at the center of a turntable so that the working chamber is parallel to the turntable surface. From rest, the table rotates and reaches to an angular velocity of 150 rpm. While rotating together with the turntable and without the activation of ion wind, the output voltage observed on hotwires by Fig. 6 depicts that the rotation does not impact on airflow and then the temperature of hotwires in the working/sensing chamber. In other words, without the ion wind, any change of environment does not impact on the present closed system.

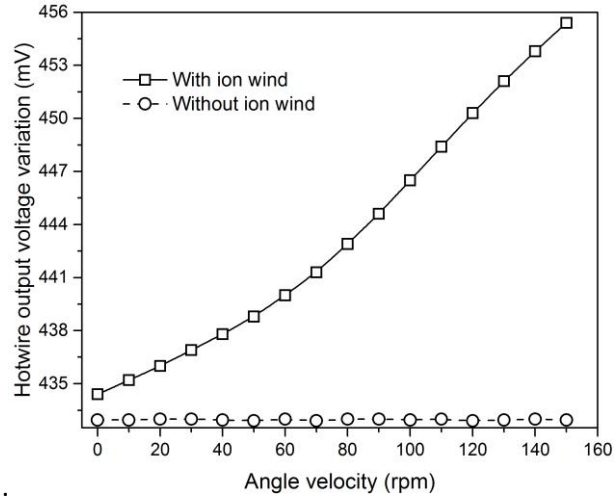

Figure 6. Experimental results: Output voltage measured on hotwires plotted versus the angular velocity of turntable under ion wind generated by an applied voltage of 2.9 kV (square line) and without the use of ion wind (circle line). Hotwires were heated by a current of 92.8mA

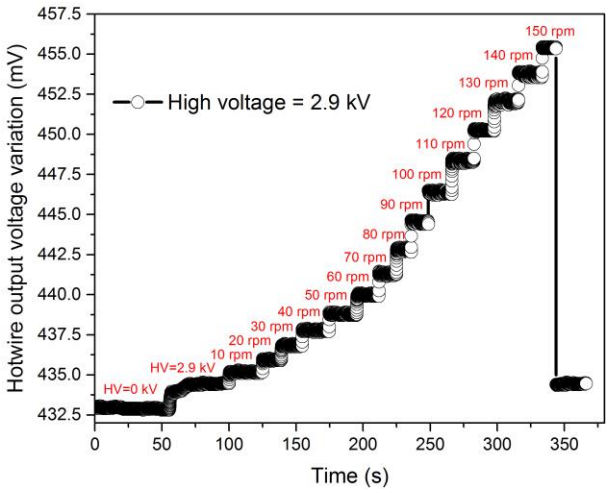

Figure 7. Time evolution of output voltages on hotwires with respect to angular rate of the turntable from rest to 150 rpm under the effect of ion wind generated by a high voltage of 2.9kV

With the turntable at rest, ion wind, which is activated by a voltage of 2.9 kV applied between pin-ring electrodes, induces an output voltage of 434.4 mV on hotwires (see Fig. 6). While the turntable rotates increasingly to reach to 150 ~~rpm~~, the Coriolis effect caused by the table's rotation deflects airflow in the working chamber. The output voltage measured on hotwire increases and achieves 455.4 mV with an estimated sensitivity of 24.08 µV/deg/sec. The deflection of airflow regularly increases with the increasing of turntable speed evidenced by the regular augmentation of the output voltage measured observed on hotwires as shown in Fig. 7. Furthermore with a given angular velocity of the turntable, the output voltage observed on hotwires does not vary, i.e. the flow deflection is stable while the turntable rotates with a constant velocity.

Experimental results by Fig. 8 show that with a given high voltage applied between pin-ring electrodes, the output voltage measured on hotwires quasi-linearly increases with the increase of the turntable's angular speed and then achieves at a maximum value before gradually decreases. For example, with an applied voltage of 2.7 kV (triangle line), the output voltage measured on hotwires increases with a scale factor of 22.03 $\mu V^0/s$ and reaches to about 13.5 mV at the turntable speed of 120 rpm before gradually decreases. This maximum value indicates that flow deflection equals to the distance from flow axis to the hotwire, $d_\omega = d_{\omega\_max}$ = 2.5 mm, i.e. a half of the distance between two opposite hotwires and can be used to estimate the average velocity of ion wind *U* using Eq. (1) as follows

$$d_{\omega\_max} = \omega_{max} L^2/U, \quad (4)$$

where ω_{max} is the yield speed of the turntable that gives highest hotwire output voltage, found by experiment and depends on the discharge voltage as depicted in Fig. 8a. Hence, with a maximum deflection of ion wind, the average velocity is determined as $U = \omega_{max}\, L^2/d_{max} = 0.24$ m/s at the discharge voltage of 2.7 kV.

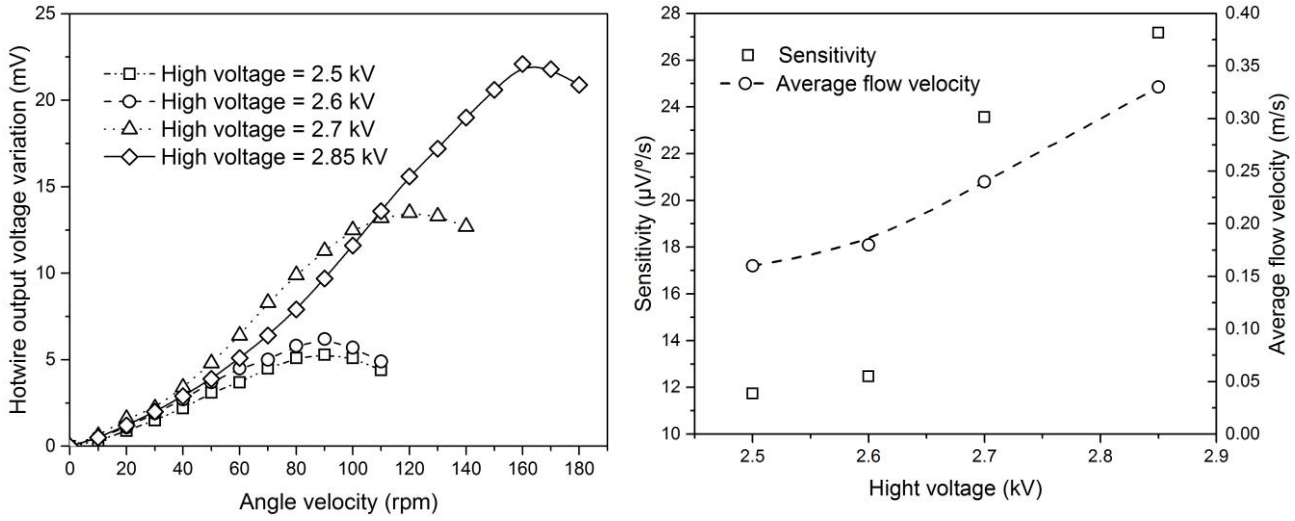

(a) (b)

Figure 8. Experimental results: a) *Variation of output voltage measured on the hotwire 1 plotted versus the angular velocity of turntable for a range of voltages from 2.5 kV to 2.85 kV applied on pin-ring electrodes;* b) *Effect of corona discharge voltage on the average velocity of ion wind (circle line) and the sensitivity of the device (square line).*

It is worth noting that since the velocity of airflow is relative to the discharge current as presented in Eq. (3), the performance of the system can be adjusted by a relevant discharge current or in other words, the corresponding discharge voltage applied on the pin electrode. This finding was demonstrated by experimental results in Fig. 8b in which the sensitivity of the device and the average velocity of ion wind *U* are plotted versus the discharge voltage. Results show that both the sensitivity and the average velocity *U* increase with the increasing of the discharged voltage.

Last but not least, the total power which includes energies consumed by the corona discharge process (2 mW), and by the high voltage circuit (15 mW), is about 17 mW. So, the energy consumption of the present device is relatively lower than one by a designed system using the conventional piezoelectric diaphragm, which requires 200 mW as quoted in [23]–[25].

3.4. Effect of linear acceleration

In order to investigate the effect of acceleration on the sensitivity of the system, the device is installed at the distance R_t = 7 cm from the center of the turntable (i.e, at the edge as shown in Fig. 9 inset). While the turntable rotates, the centripetal acceleration of the device is linear and determined as $a_C = (2\pi\omega)^2 R_t$.

While the turntable rotates from rest to 50 rpm, Fig. 9 shows the evolution of output voltages observed on hotwires with the device installed at the centre is slightly higher than that when the device is at the distance R_t from the table's centre. It can be explained as the turntable accelerates, force by the generated centripetal acceleration against the deflection of ion wind by the Coriolis force.

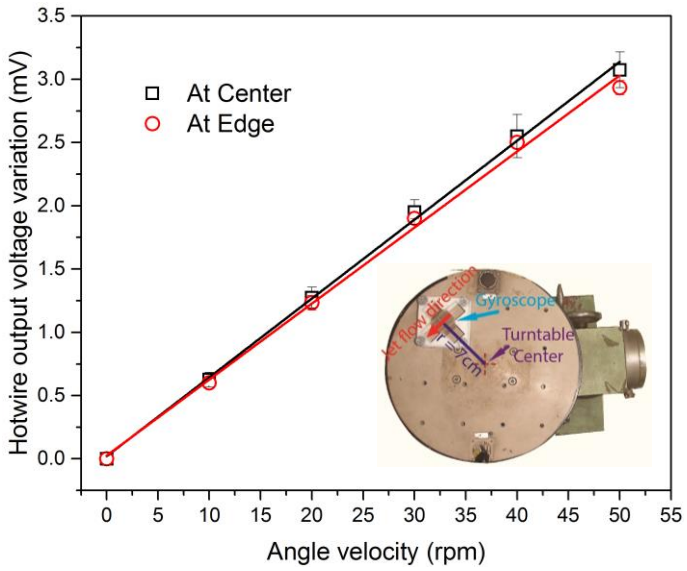

Figure 9. Effect of acceleration on sensing: Output voltage measured on hotwires plotted vs the angular speed when device is installed at the center and the edge of the turntable to impose a linear acceleration. The inset is an experimental set-up of the investigation.

In comparison with output voltages measured on hotwires of device at the turntable center, the effect of centripetal acceleration on the sensitivity of the present system is around 1.87 $\mu Vm^{-1}s^2$. Thus, the effect of centripetal acceleration can be linearly approximated as 18.34 μVg^{-1}, which is equivalent to 0.62% of the full-scale measurement as given in Fig. 9.

3.5. Symmetry of jet flow

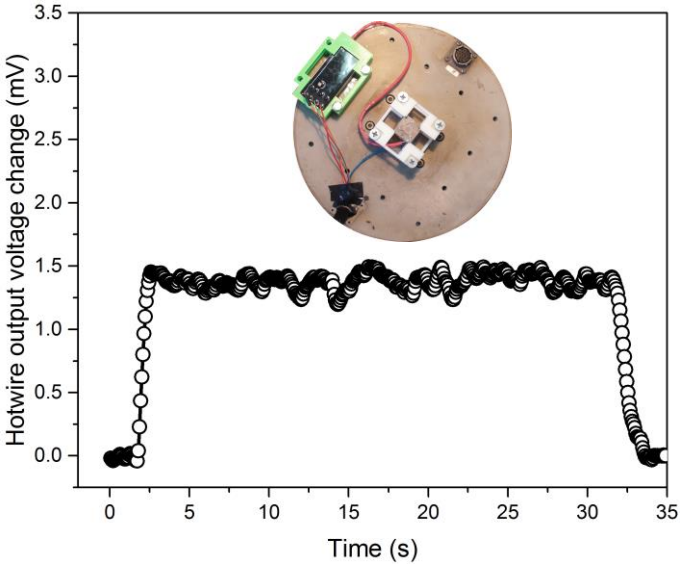

Figure 10. Time evolution of output voltage measured on hotwires with device installed vertically at the center of turntable. The inset is an experimental set-up for investigation.

The jet flow network generated within the device is highly symmetric. In order to investigate this characteristic, the device is vertically installed at the center of the turntable so that the rotational axis is coincident to the axis of working chamber. Thus, while the turntable rotates, the jet flow in the working chamber regularly spins about its axis. Hence, the velocity of airflow going through hotwires is the same, i.e $\vec{\omega} \times \vec{U} \approx 0$. This is confirmed by the experimental results presented in Fig. 10 in which the turntable rotates

from rest and reaches to 110 rpm and ion winds are activated by a discharge voltage of 2.5 kV. At the stable angular velocity of 110 rpm, the variation of output voltage measured on hotwires was pretty small, around ± 100 μV. It means that the jet flow in working chamber is coincident about its axis, therefore the relative cooling on hotwires is insignificant by the curling of airflow caused the turntable's rotation [26].

4. Conclusions

We have designed, developed and evaluate the characteristics of jet flow gyroscope using pin-ring electrodes based ion wind corona discharge method. For the present device, the deflection of jet flow by the Coriolis force due to the angular rate is detected with a sensitivity of 24.08 μV/º/s using an applied voltage of 2.9 kV to activate ion winds and a current of 100 mA to heat hotwires. The device is robust owing not to require any vibrating component in the new structure. Furthermore, due to low energy consumption, the present gyroscope can work with a small battery. Finally, this work is a valuable contribution in developing new sensing techniques and the manufacturing of fluidics for multidisciplinary areas such as microfluidics and fluidic multiplier.

Reference

[1] N.-C. Tsai, J.-S. Liou, C.-C. Lin, and T. Li, "Suppression of dynamic offset of electromagnetic drive module for micro-gyroscope," *Mech. Syst. Signal Process.*, vol. 25, no. 2, pp. 680–693, Feb. 2011.

[2] H. Cao, H. Li, J. Liu, Y. Shi, J. Tang, and C. Shen, "An improved interface and noise analysis of a turning fork microgyroscope structure," *Mech. Syst. Signal Process.*, vol. 70–71, pp. 1209–1220, Mar. 2016.

[3] H. Cao *et al.*, "Sensing mode coupling analysis for dual-mass MEMS gyroscope and bandwidth expansion within wide-temperature range," *Mech. Syst. Signal Process.*, vol. 98, pp. 448–464, Jan. 2018.

[4] V. T. Dau, T. X. Dinh, and S. Sugiyama, "A MEMS-based silicon micropump with intersecting channels and integrated hotwires," *J. Micromechanics Microengineering*, vol. 19, no. 12, p. 125016, Dec. 2009.

[5] Z. Zhang, J. Kan, S. Wang, H. Wang, J. Wen, and Z. Ma, "Flow rate self-sensing of a pump with double piezoelectric actuators," *Mech. Syst. Signal Process.*, vol. 41, no. 1–2, pp. 639–648, Dec. 2013.

[6] V. T. Dau and T. X. Dinh, "Numerical study and experimental validation of a valveless piezoelectric air blower for fluidic applications," *Sensors Actuators B Chem.*, vol. 221, pp. 1077–1083, Jul. 2015.

[7] V. T. Dau, D. V. Dao, T. Shiozawa, H. Kumagai, and S. Sugiyama, "Development of a dual-axis thermal convective gas gyroscope," *J. Micromechanics Microengineering*, vol. 16, no. 7, pp. 1301–1306, Jul. 2006.

[8] V. T. Dau, D. V. Dao, T. Shiozawa, H. Kumagai, and S. Sugiyama, "A Single-Axis Thermal Convective Gas Gyroscope," *Sensors Mater.*, vol. 17, no. 8, pp. 453–463, 2005.

[9] T. X. Dinh and Y. Ogami, "A Principle to Generate Flow for Thermal Convective Base Sensors," *J. Fluids Eng.*, vol. 131, no. 4, p. 041401, Apr. 2009.

[10] K. Takemura, S. Yokota, M. Suzuki, K. Edamura, H. Kumagai, and T. Imamura, "A liquid rate gyroscope using electro-conjugate fluid," *Sensors Actuators A Phys.*, vol. 149, no. 2, pp. 173–179, 2009.

[11] S. Liu and R. Zhu, "Micromachined Fluid Inertial Sensors," *Sensors*, vol. 17, no. 2, p. 367, Feb. 2017.

[12] J. Bahari, R. Feng, and A. M. Leung, "Robust MEMS Gyroscope Based on Thermal Principles," *J. Microelectromechanical Syst.*, vol. 23, no. 1, pp. 100–116, Feb. 2014.

[13] V. T. Dau, T. X. Dinh, C. D. Tran, T. T. Bui, and H. T. Phan, "A study of angular rate sensing by corona discharge ion wind," *Sensors Actuators, A Phys.*, vol. 277, pp. 169–180, 2018.

[14] T. M. Dauphinee, "Acoustic Air Pump," *Rev. Sci. Instrum.*, vol. 28, no. 6, p. 452, Dec. 1957.

[15] V. T. Dau, T. X. Dinh, T. T. Bui, and C. D. Tran, "Vortex flow generator utilizing synthetic jets by diaphragm vibration," *Int. J. Mech. Sci.*, vol. 142–143, no. May, pp. 432–439, 2018.

[16] E. P. Mednikov, B. G. Novitskii, E. P. Mednikov, and B. G. Novitskii, "Experimental study of intense acoustic streaming," *Akust. Zhurnal*, vol. 21, pp. 245–249, 1975.

[17] K. D. Dorfman, M. Chabert, J.-H. Codarbox, G. Rousseau, P. de Cremoux, and J.-L. Viovy, "Contamination-free continuous flow microfluidic polymerase chain reaction for quantitative and clinical applications.," *Anal. Chem.*, vol. 77, no. 11, pp. 3700–4, Jun. 2005.

[18] J. Atencia and D. J. Beebe, "Steady flow generation in microcirculatory systems.," *Lab Chip*, vol. 6, no. 4, pp. 567–74, Apr. 2006.

[19] T. X. Dinh, D. B. Lam, C. D. Tran, T. T. Bui, P. H. Pham, and V. T. Dau, "Jet flow in a circulatory miniaturized system

using ion wind," *Mechatronics*, vol. 47, no. September, pp. 126–133, Nov. 2017.
[20] N. T. Van *et al.*, "A Circulatory Ionic Wind for Inertial Sensing Application," *IEEE Electron Device Lett.*, vol. 40, no. 7, pp. 1182–1185, Jul. 2019.
[21] M. Robinson, "Movement of air in the electric wind of the corona discharge," *Trans. Am. Inst. Electr. Eng. Part I Commun. Electron.*, vol. 80, no. 2, pp. 143–150, 1961.
[22] L. Li, S. J. Lee, W. Kim, and D. Kim, "An empirical model for ionic wind generation by a needle-to-cylinder dc corona discharge," *J. Electrostat.*, vol. 73, pp. 125–130, 2015.
[23] V. T. Dau, T. X. Dinh, and T. T. Bui, "Jet flow generation in a circulatory miniaturized system," *Sensors Actuators B Chem.*, vol. 223, pp. 820–826, 2015.
[24] H. T. Phan, T. X. Dinh, and V. T. Dau, "Development of a jet-generator and its application to angular rate sensor," in *2015 China Semiconductor Technology International Conference*, 2015, pp. 1–3.
[25] L. Murata Manufacturing, "Piezoelectric Diaphragms, Murata Manufacturing Co., Ltd.," 2016. [Online]. Available: http://www.murata.com/en-sg/products/sound/diaphragm.
[26] P. T. Hoa, T. X. Dinh, and V. T. Dau, "Design Study of Multidirectional Jet Flow for a Triple-Axis Fluidic Gyroscope," *IEEE Sens. J.*, vol. 15, no. 7, pp. 4103–4113, Jul. 2015.